Multi-proxy speleothem-based reconstruction of mid-MIS 3 climate in South Africa

Jenny Maccali[1,2], Anna Nele Meckler[1,2], Stein-Erik Lauritzen[1,2], Torill Brekken[3], Helen Aase Rokkan[3], Alvaro Fernandez[4], Yves Krüger[3], Jane Adigun[5], Stéphane Affolter[6], Markus Leuenberger[7]

[1]Department of Earth Sciences and Bjerknes Centre for Climate Research, University of Bergen, Bergen, N-5007, Norway
[2]SFF Centre for Early Sapiens Behaviour (SapienCE), University of Bergen, Bergen, N-5020, Norway
[3]Department of Earth Sciences, University of Bergen, Bergen, N-5007, Norway
[4]Andalusian Institute of Earth Sciences, University of Granada, Granada, 18100, Spain
[5]Department of Anthropology and Archaeology, University of South Africa, Pretoria, 0002, South Africa
[6]Department of Environmental Sciences, University of Basel, Basel, 4056, Switzerland
[7]Climate and Environmental Physics Division, Physics Institute and Oeschger Centre for Climate Change Research, University of Bern, Bern, 3012, Switzerland

Correspondence to: Jenny Maccali (jenny.maccali@uib.no)

Abstract. The southern coast of South Africa displays a highly dynamical climate as it is at the convergence of the Atlantic and Indian Ocean, and it is located near the subtropical/temperate zone boundary with seasonal influence of easterlies/westerlies. The region hosts some key archeological sites with records of significant cognitive, technological and social developments. Reconstructions of the state and variability of past climate and environmental conditions around sites of archeological significance can provide crucial context for understanding the evolution of early humans. Here we present a short but high-resolution record of hydroclimate and temperature in South Africa. Our reconstructions are based on trace elements, calcite and fluid inclusion stable isotopes, and fluid inclusion microthermometry from a speleothem collected in Bloukrantz Cave, in the De Hoop Nature Reserve in the Western Cape region of South Africa.

Our record covers the time period from 48.3 to 45.2 ka during Marine Isotope Stage 3. Both $\delta^{18}O_c$ and $\delta^{13}C_c$ show strong variability and covary with Sr/Ca. This correlation suggests that the control on these proxies originates from internal cave processes such as prior carbonate precipitation, which we infer to be related to precipitation amount. The hydroclimate indicators suggest a shift towards overall drier conditions after 46 ka, coincident with a cooling in Antarctica and drier conditions in the eastern part of South Africa corresponding to the Summer Rainfall Zone.

Fluid inclusion-based temperature reconstructions show good agreement between the oxygen isotope and microthermometry methods, and results from the latter display little variation throughout the record, with reconstructed temperatures close to the present-day cave temperature of 17.5 °C. Overall, the BL3 record thus suggests relatively stable temperature from 48.3 to 45.2 ka whereas precipitation was variable with marked drier episodes on sub-millennial timescales.

1 Introduction

45 The southern region of South Africa is a key region for the study of human evolution. Some scholars have linked episodes of significant cultural changes, seemingly not related to subsistence requirements, during the Middle Stone Age (MSA) with artifacts such as engraved ochre, an ochre processing kit, engraved ostrich eggshells, bifacial points, and perforated marine shell beads, which are considered archaeological markers for 'symbolically mediated behavior' (e.g. Henshilwood et al., 2011; Henshilwood et al., 2014; Marean et al., 2007; Wurz, 2002). The environmental conditions at the time have been suggested to

50 drive changes either by offering refuge (suitable habitat) allowing for experimentation, or on the contrary, by forcing innovative mechanisms of adaptation (d'Errico, 2003; Wadley, 2021). However, although the number of paleoenvironmental reconstructions in South Africa's southern Cape coastal region during the MSA is increasing (e.g. Bar-Matthews et al., 2010; Braun et al., 2019b; Braun et al., 2020; Chase, 2010; Chase et al., 2021; Strobel et al., 2022), information on past climate in this region still remains sparse. In this study, we apply a suite of traditional and novel approaches to reconstruct climate in

55 South Africa from a speleothem from Bloukrantz cave, that grew during a short interval during Marine Isotope Stage (MIS) 3. Our goal is to cross-validate the various proxies and reconstruct the state and variability of hydroclimate and temperature.

Today, South Africa's climate is marked by different seasonal and spatial rainfall patterns (Fig. 1). During austral winter, the southern westerlies wind belt is displaced northward, bringing precipitation to the southwestern tip of South Africa (the Winter Rainfall Zone – WRZ). During austral summer, the westerlies are displaced southwards, allowing easterlies to bring rain to

60 the eastern part of South Africa (the Summer Rainfall Zone – SRZ). Bloukrantz Cave and several key archeological sites are located in the junction of these two rain zones, known as the Year-round Rainfall Zone (YRZ), with winter rain accounting for 30 – 60 % of the annual precipitation and no marked seasonality (Carr et al., 2006; Chase and Meadows, 2007; Roffe et al., 2019). Identifying the drivers of climate change in the YRZ is not straightforward as the YRZ is a transition zone between WRZ and SRZ and thus influenced by a variety of mechanisms: Indian Ocean sea surface temperature (SST), convective and

65 tropical weather systems in the east (Engelbrecht et al., 2015), and the westerlies belt position and intensity, along with the associated frontal systems, in the west (Chase, 2010; Chase and Meadows, 2007).

MIS 3, the period between ~ 60 to 29 ka during the last glacial period, is characterized by a global mean sea level lower than today (Siddall et al., 2008) and globally colder temperature (Van Meerbeeck et al., 2009). Northern hemisphere ice core proxies reveal substantial millennial-scale variability such as Dansgaard-Oeschger and Heinrich events (Andersen et al., 2004) and

70 associated temperature changes (Huber et al., 2006; Kindler et al., 2014). In the Southern Hemisphere, Antarctic ice core records display similar variability, though of a lesser amplitude (Siddall et al., 2008). The Antarctic ice core record is mimicked by SST reconstructions from sediment cores surrounding the southern tip of the African continent, both in the Indian (e.g. Simon et al., 2013) and the Atlantic sector (e.g. Dyez et al., 2014; Peeters et al., 2004). Mean annual precipitation reconstructions in the SRZ of Southern Africa closely follow solar radiation intensity (daily January insolation at 30°S) with

75 reduced amplitude variation during MIS 3 compared to MIS 4 and 5 (Partridge et al., 1997). This is illustrated in a speleothem sample from Wolkberg cave, where a drying trend was recorded from ~51 to 46 ka and linked to decreasing solar radiation

(Holzkämper et al., 2009). In the YRZ, fynbos pollen numbers indicate a drying period from 60 to 40 ka followed by wetter conditions from 40 to 30 ka (Quick et al., 2016). In the speleothem record, this is illustrated by a marked decrease in the overall number of speleothem samples recovered at ~60 ka, followed by a slight increase from 45 to 30 ka (Braun et al., 2019a). In the Little Karoo region, still within the YRZ, a composite record (Chase et al., 2021; Talma and Vogel 1992) shows evidence of a shift from low- to high-latitude forcing dominance at the onset of MIS 4 (~70 ka). In the composite record (Chase et al., 2021), changes in δ^{13}C have been interpreted to reflect changes in rain dominance, with increased summer rain dominance from 59 to 54 ka, from 49 to 47 ka and from 41 to 36 ka. A speleothem from the same region, covering the 88 – 18 ka time interval, displays trends similar to terrestrial runoff from the Namibian west coast, suggesting a general dominant contribution of winter rains (Braun et al., 2020). Finally, aridity reconstructions indicate variable aridity conditions in the WRZ through MIS 3, although with overall drier conditions compared to MIS 4 (Stuut et al., 2002).

Speleothems are cave deposits (most often Ca carbonates), which can be accurately dated by the U-Th method. They are most commonly used to reconstruct changes in precipitation on the basis of variations in the oxygen isotopic composition (δ^{18}O) of the calcite matrix (Lachniet, 2009). The carbon isotopic composition (δ^{13}C) of speleothem calcite is more complex to interpret, as it can reflect changes in vegetation (C3 vs C4 plants) and respiration processes above the cave and/or cave internal processes leading to C isotope fractionation (Fohlmeister et al., 2020). The latter are commonly also reflected in variations in trace element to Ca ratios, such as Mg/Ca or Sr/Ca (Stoll et al., 2012). Here we combine both δ^{18}O and δ^{13}C from the calcite (later noted with subscript c), and Sr/Ca ratios to infer past changes in precipitation.

Recently, quantitative proxies for cave temperature have been developed (Affek et al., 2008; Blyth and Schouten, 2013; Kluge et al., 2008; Krüger et al., 2011; Vonhof et al., 2006). Cave temperature generally reflects the mean annual air temperature outside of the cave (Poulson and White, 1969), making cave deposits ideal candidates for land temperature reconstructions. The first quantitative temperature reconstruction method that has been proposed is the water-carbonate paleothermometer based on oxygen isotopes. The theoretical background of this approach dates back to the 1950s (Epstein et al., 1951; Epstein et al., 1953; Mccrea, 1950; Urey, 1947). In speleothems, however, the application of this thermometer has initially been limited by the lack of knowledge of the water isotopic composition. This information can now be gained from fluid inclusion water isotope (FIWI) measurements (e.g. Affolter et al., 2014; Fernandez et al., 2023; Matthews et al., 2021; Vonhof et al., 2006; Warken et al., 2022; Wassenburg et al., 2021; Wortham et al., 2022), which reveal the isotopic composition of former drip water preserved in microscopic inclusions in the speleothem calcite. Here we combine temperature estimates based on the difference in oxygen isotopic composition of fluid inclusions and calcite with another, independent temperature proxy, namely fluid inclusion microthermometry. The microthermometry approach uses liquid-vapor homogenization temperatures to determine the density of the enclosed drip water (Krüger et al., 2011; Løland et al., 2022). The suite of all methods applied here allows us to derive multi-proxy records of both hydroclimate and temperature.

2 Material and Methods

2.1 Site description and setting

Bloukrantz Cave (34°27.557'S, 20°46.697'E, 10-25 m a.s.l.) is located at the coast of South Africa in the De Hoop Nature reserve in the southern Cape region (Noah, 2011). The cave is a composite marine abrasion cave formed in quartzite where the entrance is almost completely closed by travertine derived from overlying, aeolian calcarenite dunes. The narrow entrance leads to a first chamber followed by a steep slope down to the main room (Fig. S1). The interior of the cave is largely filled with columnar stalagmites that have grown since the entrance wall closed the cave. The speleothem used in this study (BL3) was collected in a smaller chamber adjacent to the main room (Adigun, 2016). The cave floor mainly consists of sand mixed with bat guano. An Onset HOBO U23-001 ProV2 temperature logger was placed in the cave in February 2018 and data were collected in January 2019 and March 2020. In 2018, dripping was not active, and the logged relative humidity (rH) was ~90%. During the two subsequent visits in January 2019 and March 2020, dripping in the cave was active and the logged rH was ~100% (Fig. S2). Temperature in the cave was fairly stable between February 2018 and March 2020 and varied from 16.4 to 18.8 °C with a mean temperature of 17.5 ± 0.5°C (±1SD). Slightly further inland, at the Potberg station (34°22.623'S, 20°02.044'E, 176 m a.s.l.), the mean annual temperature was 16 ± 5 °C for the same period with annual precipitation of 220-380 mm. At Klipdrift sea cave (34°27.096'S, 20°43.458'E), a few kilometers west along the coast, a mean annual temperature of 17.6 ± 0.3 °C (±1SD) was recorded. The similar temperatures recorded at the two sites allow us to exclude potential warming from guano degradation at Bloukrantz cave as the Klipdrift sea cave does not shelter a bat colony. Bloukrantz cave is ideally positioned in the YRZ to provide local paleoclimate reconstructions in relation with key archeological sites such as Blombos cave and Klipdrift shelter.

2.2 Sample description

Sample BL3 (Figs. 2, S3) is 425 mm long and 105 mm wide at its widest (close to mid-height). The stalagmite displays two distinct growth episodes with a clear hiatus at 198 mm from the top (Fig. S3). The pre-hiatus part consists of white milky calcite with microcrystalline fabric according to the classification scheme of (Frisia, 2015) and displays multiple changes of the direction of the stalagmite growth axis, most likely linked to lateral shifts of the dripping site. After the hiatus, stalagmite BL3 features a 100 mm long straight section of translucent calcite with brittle columnar fabric (Frisia, 2015) that also covers the flanks of the lower part (Fig. S4). The top 95 mm consist again of microcrystalline, milky calcite, and shows clear layering. In this study, we are focusing mainly on the lower part of BL3 that formed during MIS 3 while the upper part formed during the Holocene. The clear growth axis changes observed at 241, 292, 312, 354, 380, and 401 mm (dashed lines in Fig. 2) are associated with darker layers. The surfaces of these dark layers show slight dissolution features and indicate potential short-term growth interruptions of the stalagmite (S. Frisia, personal communication).

Apart from these dark hiatus layers, inspections of thin sections did not reveal any significant changes of the calcite fabric throughout the MIS 3 part of the sample. The orientation of the calcite crystals in the microcrystalline fabric does not exhibit

preferential crystallographic orientation, which is indicated by the tipped terminations of small intra-crystalline fluid inclusions. The calcite fabric as a whole is quite porous, which explains its milky appearance. Fluid inclusions, both intra- and inter-crystalline, are abundant but of small size. A large portion of the inclusions is two-phase containing liquid water and a gas bubble. It is not yet clear whether the gas bubble contains air that might have been trapped during the formation of inclusions, or water vapor that would rather indicate post-formation water loss or volume alteration of the inclusions. Mono-phase liquid inclusions, in contrast, were found to be relatively sparse.

2.3 Sample preparation

The sample was cut lengthwise into 1 cm thick slabs. One slab was used for X-ray Fluorescence (XRF) scanning while a second slab cut form the other half of the stalagmite was used for dating, isotopic analyses, and microthermometry analyses. Since stable isotopes and trace elements were measured on different slabs, the Sr/Ca and the stable isotopes transects show slight offsets which can be accounted for by tracing visible layers in both slabs (grey bars in Fig. 2 connect equivalent features).

2.3.1 U-Th dating

Subsamples for dating were drilled using a Sherline 5410 milling stage mounted with a 1.5 mm drill bit. The chemical separation procedure was largely derived from Edwards (1988). Briefly, ~250 µg of carbonate powder was spiked using a mixed solution of ^{229}Th-^{233}U-^{236}U, calibrated using a Harwell uraninite (HU-1) solution considered at secular equilibrium. After dissolution with concentrated HNO_3, Fe-precipitates were formed by addition of clean Fe and stepwise addition of NH_4OH. After centrifugation the Fe-precipitate was dissolved in HCl and loaded onto AG1X8 resin, where Th was separated from U. Each fraction was then purified by another pass through AG1X8 resin for Th and U-TEVA resin for U. Isotopic ratios were measured at the Department of Earth sciences at the University of Bergen in dry plasma mode on a Nu Plasma II instrument upgraded with a plasma 3 source. Isotopic ratios were measured by peak jumping on a secondary electron multiplier (SEM). Mass bias was corrected using the ^{236}U/^{233}U spike ratio. A HU-1 solution was used as a standard solution to monitor analytical sessions. Activity ratios were calculated using decay constant values from Cheng et al. (2013). Ages were calculated using the Excel Isoplot add-in 3.75 (Ludwig, 2003) without decay constant uncertainties. All U-series data reported in tables and figures are presented with a ±2SD uncertainty. The ^{232}Th/^{238}U bulk Earth ratio of 3.8 was used to correct ^{230}Th ages for detrital Th contamination (Taylor and Mclennan, 1985). Two samples were additionally dated at the Isotope Laboratory at Xi'an Jiaotong University (see supplement).

2.3.2 Trace elements

Sr/Ca ratios can be rapidly obtained by non-destructive XRF scanning (Scroxton et al., 2018). For this study, Sr/Ca ratios were measured on an ITRAX XRF core scanner from Cox Analytical Systems (Gothenburg, Sweden) using a 3 kW molybdenum (Mo) X-ray tube. The voltage was set to 28 kV, current to 28 mA, resolution to 200 µm, and exposure time to 20 s (Rokkan, 2019). The slab on which the XRF scanning was performed was further cut in smaller pieces and placed onto a flat plexiglass

support inserted on top of the rail system. The stalagmite pieces were rotated so that the scans were taken parallel to the growth axes. The data presented here are the average of three parallel scans performed a few mm apart.

2.3.3 Calcite stable isotopes

Using the milling stage, carbonate powder was milled continuously in 1mm increments along transects following the growth axis of the BL3. Oxygen and carbon isotope ratios were measured on 30-50 µg samples following routine protocols at Farlab (Facility for advanced isotopic research and monitoring of weather, climate and biogeochemical cycling) on a Thermo Fisher Scientific MAT253 isotope ratio mass spectrometer with a Kiel IV carbonate preparation device. The $\delta^{13}C_c$- and $\delta^{18}O_c$-values were calibrated against an in-house marble standard and NBS18, and are expressed in ‰ against VPDB. Reproducibility of standard measurements was better than 0.10 ‰ (1SD) for $\delta^{18}O$ and better than 0.05 ‰ (1SD) for $\delta^{13}C$.

2.3.4 Microthermometry (liquid-vapor homogenization temperatures)

The microthermometric approach uses the density of water in stalagmite fluid inclusions as a proxy to reconstruct cave temperature. The application of the microthermometry method to fluid inclusions in stalagmites is described in detail by Krüger et al. (2011) and sample preparation is described in Løland et al. (2022). Briefly, blocks of 20 mm width and 30-40 mm length were cut from the second slab alongside the isotope transects. Then, ~300 µm thick sections were cut from the calcite blocks with a low-speed saw (Buehler Isomet), and these unpolished thick sections were broken into smaller pieces of ~4x4 mm to fit on the sample holder of the microscope heating/freezing stage (Linkam THMS600). Individual monophase fluid inclusions were selected for analysis and cooled to 5 °C. At this temperature, the inclusion water is in a metastable liquid state and a femtosecond laser pulse was used to nucleate a vapor bubble (Krüger et al., 2007). Upon subsequent heating the vapor bubble becomes progressively smaller and eventually disappears at the liquid-vapor homogenization temperatures ($T_{h(obs)}$). The measured $T_{h(obs)}$ values were then corrected for surface tension effects using an additional measurement of the vapor bubble radius at known temperature and a thermodynamic model (Marti et al., 2012) to calculate the water density and thus the formation temperature of the fluid inclusion. Information on the original density of the former drip water can be obtained only from monophase liquid fluid inclusions. Measurements of $T_{h(obs)}$ and of the bubble radii were challenging because of the small size of the inclusions (100 - 3000 µm³). In some cases, the collapse of the vapor bubble at $T_{h(obs)}$ could not be observed directly. In these situations, a temperature cycling procedure with stepwise heating and subsequent cooling was applied to determine the homogenization temperature precisely. Bubble images for the radius measurements were taken at 5.1 °C where the vapor bubble in a calcite confined system reaches maximum size. Between 5 to 20 inclusions were measured in triplicate for each layer, depending on the number and size of available inclusions. Mean temperatures of coeval inclusions from the same growth layers were considered as a best estimate of the stalagmite formation temperature at the respective sample position. Temperature uncertainties are reported as 2 standard error (SE) of the mean.

2.3.5 Fluid inclusion water isotopes

The remaining part of the blocks was divided in 3-5 mm wide lamella cut along the curved stalagmite growth layers using a diamond wire saw (Well 3421). These layer-parallel samples were then split into coeval subsamples of about 0.2-0.4 g for replicate measurements of fluid inclusion water isotopes. A total of 31 layers were analyzed, 25 at Farlab in Bergen and 6 at the University of Bern. The analytical setup in Bergen is described by Sodemann et al. (2023). Briefly, aliquots of >100 mg were crushed in a heated (120 °C) crusher device (similar to that described by e.g. De Graaf et al., 2020) connected to a Picarro L2130-i laser spectrometer. A microdrop device ensures a stable humidity background in the air stream that purges the crusher. After loading the sample into the preheated crusher, it took about 15-20 minutes to achieve a stable water background in the system. The fluid inclusion water was then released by crushing the sample and its isotopic composition was determined by subtracting the water background from the signal (Affolter et al., 2014). The analytical setup in Bern is described in Affolter et al. (2014).

FIWI analyses could be performed only in the MIS 3 part of the stalagmite and on the topmost layers, because water yields from the columnar fabric of the Holocene part were too low. Data accuracy and reproducibility were estimated using in-house water standards sealed in borosilicate capillaries and crushed in the analytical line. Reproducibility was <0.4 ‰ for $\delta^{18}O$ and <1.2 ‰ for δ^2H (± 1SD). Results are reported as the average of 3 replicates per layer and uncertainties are calculated as 1SD, or set as 0.4 ‰ for $\delta^{18}O_w$ and 1.2 ‰ for δ^2H_w, whichever was larger. FIWI temperatures were calculated using the empirical relationship from Tremaine et al. (2011), with the $\delta^{18}O_c$ measured on the crushed carbonate remaining after water isotope analyses. Uncertainties are reported as ±1 SD and include error propagation of both water and calcite $\delta^{18}O$.

3 Results

3.1 U-Th dating and Age model

A total of 21 dates were obtained and range from 1.29 ± 0.01 to 47.54 ± 0.37 ka (see supplementary material). Two dates (at 428 and 339 mm) were rejected as clear outliers. The age-depth model was calculated using the StalAge algorithm in R (Scholz and Hoffmann, 2011) as two distinct sections, before and after the hiatus, and is reported with a 95% confidence interval. The two dates performed at the Isotope Laboratory at Xi'an Jiaotong University have been included in the age-depth model. The age-depth model (Fig. S5) displays an almost linear growth from 48.4 to 45.2 ka with an average growth rate of 0.07 mm/yr except from ~46.0 to 46.4 ka when the growth appeared to have been faster with an average growth rate of 0.19 mm/a. After the hiatus, the growth was slower from 7.6 to 3.6 ka (0.06 mm/a) and faster from 3.6 to 1.5 ka (0.09 mm/a).

3.2 Trace elements

The Sr/Ca count ratios range from 288 to 687 (Fig. 2 and Fig. S6). For the lower part (MIS 3 section), a series of positive excursions of variable amplitude are overprinted on the baseline signal. The baseline itself increases slightly from 432 to 260 mm (48.4 to 46 ka), followed by a more pronounced increase after 260 mm (46 ka).

After the hiatus (Holocene section), the Sr/Ca signal drops markedly with an average value of 348 between 200 and 150 mm (7.6 to 3.5 ka), followed by a gradual increase between 150 to 90 mm (3.5 to 2.9 ka) to values of 500. From 90 mm towards the top of the stalagmite (2.9 to 1.5 ka) values remain high with large variability. The Holocene section is characterized by an overall higher frequency variability.

3.3 Calcite stable isotopes

Bottom (MIS 3) and top (Holocene) part $\delta^{18}O_c$ values range from -3.7 to -1.0 ‰ and from -5.1 to -2.6 ‰, respectively. $\delta^{13}C_c$ values range from -7.9 to -1.4 ‰ for the bottom (MIS) 3 part and from -8.6 to -2.6 ‰ in the top (Holocene) section. $\delta^{18}O_c$ and $\delta^{13}C_c$ closely follow the same pattern. As with the Sr/Ca record, the isotopic baseline of the bottom (MIS 3) section displays little variation from 432 to 260 mm (48.4 to 46 ka) followed by an increase after 260 mm (46 ka) of up to 1 ‰ in $\delta^{18}O_c$ and 3 ‰ in $\delta^{13}C_c$. A series of peaks is superimposed on the baseline in both the $\delta^{18}O_c$ and $\delta^{13}C_c$ records and corresponds to similar peaks in the Sr/Ca signal and the presence of dark layers in the sample. The amplitude of these excursions varies from 0.9 to 1.7 ‰ for $\delta^{18}O_c$ and from 2.3 to 5.1 ‰ for $\delta^{13}C_c$. The top (Holocene) part displays lower values in both $\delta^{18}O_c$ and $\delta^{13}C_c$ immediately after the hiatus with little variation until 150 mm (3.5 ka), followed by a gradual increase until 90 mm (2.9 ka) and high values throughout the rest of the record.

3.4 Microthermometry

A total of 17 layers were analyzed including one in the Holocene part for comparison with the present-day temperature. Stalagmite formation temperatures reconstructed from the topmost Holocene part of BL3 (microcrystalline fabric), dated at 1.8 ka, indicate an average value of 17.6 ± 0.6 °C (2SE), which is close to the present-day cave temperature (17.5 ± 0.5 °C) derived from cave monitoring. Most samples display slightly skewed (towards either low or high values) Gaussian-like distributions and a scatter of the temperature data within the individual layers ranging between 3-6 °C (see Fig. S7). Some samples, however, show a larger range (7-9 °C) with semi-uniform (i.e., flatter) distributions and larger standard error of the mean; nonetheless, these samples provided mean temperatures similar to adjacent samples with smaller ranges (Fig. S5). Standard errors of the mean range from 0.5 to 2.0 °C. The considerably larger errors compared to the study of Løland et al. (2022) are, at least partly, due to the lower number T_h measurements. In general, the reconstructed temperatures are similar throughout the MIS 3 part of the stalagmite (Fig. 3 and Fig. S7), ranging from 17.7 ± 1.1 °C to 20.7 ± 1.3°C (2 SE). Apparent differences between data points are within error and therefore not interpreted here. That being said, the temperature record at face value suggests more variability from 46.5 until 45.3 ka with the highest temperature determined at ~45.8 ka (Fig. 3 and Fig. S7). The average temperature observed in the MIS3 part is 18.8 ± 0.5 °C (mean and standard deviation across all average temperatures)

3.5 Fluid inclusion water isotopes

The FIWI data are distributed in two clusters in a cross-plot of δ^2H_w versus $\delta^{18}O_w$ (Fig. 4). The older cluster comprises samples from the base of BL3 to ~46 ka and plots along the local meteoric water line (LMWL – from GNIP station at Cape Town airport from 1961 to 2013) with values ranging from -3.8 to -2.4 ‰ and from -17.4 to -10.2 ‰ for $\delta^{18}O_w$ and δ^2H_w, respectively. Samples younger than ~46 ka plot as a distinct cluster, slightly off the LMWL, and with higher values ranging from -1.0 to -0.5 ‰ and from -4.7 to -2.0 ‰ for $\delta^{18}O_w$ and δ^2H_w, respectively. Timeseries of both $\delta^{18}O_w$ and d^2H_w display trends similar to the $\delta^{18}O_c$ baseline with little variations from 48.3 to 46 ka followed by an increase after 46 ka (Fig. 3).

There are three possible ways of calculating cave temperature based on the available dataset. The first method is by estimating today's δ^2H relationship to temperature and applying it to the past considering this relationship has not significantly changed over time (e.g. Affolter et al., 2019). At Mossel bay (east of Bloukrantz Cave in the YRZ), Braun et al. (2017) found that there is a weak correlation (R=0.4) between δ^2H and temperature (δ^2H=2.7(±0.6)*T-54(±10)). Applying this relationship results in temperature estimates 4-5°C lower than microthermometry and standard deviations >4°C (1SD). The second approach is to calculate $\delta^{18}O_w$ from the measured δ^2H_w using a modern $\delta^{18}O_w$ vs δ^2H_w relationship (i.e. LMWL), and then calculating the temperature using the Tremaine et al. (2011) equation (e.g. Meckler et al., 2015). This approach is often favored as δ^2H_w is less impacted than $\delta^{18}O_w$ by fractionation processes in the cave or analytical system. It relies, however, on the assumption that the LMWL has not changed significantly over time. At Bloukrantz cave this approach results in FIWI temperature on average ~4°C lower than microthermometry and larger standard deviations compared to the third approach (Fig. S8). The third approach is to calculate temperatures using the equation of Tremaine et al. (2011) with measured $\delta^{18}O_c$ and $\delta^{18}O_w$. The calculated temperatures range from 15.4 to 21.1 °C from 48.3 to 46 ka and are in good agreement with liquid-vapor homogenization temperatures (Fig. 3 & S8) with the exception of the peaks in $\delta^{18}O_c$ where FIWI temperatures are ~3°C colder. This last approach is the one we selected as we believe it is the most likely to render actual temperature variation in the cave. After 46 ka, FIWI temperatures depart from the microthermometry results with positive offsets of 5 to 15 °C. d-excess values are fairly constant throughout the record with an average value of 9.7 ± 1.9 (1SD), except for the younger samples that display decreasing values starting at ~46 ka (Fig. S9).

4 Discussion

4.1 Hydroclimate

Interpreting isotopic and geochemical proxies in speleothems is not straightforward as epikarst and cave processes, directly or indirectly linked to climate, can alter the proxy signals (e.g. Fairchild and Baker, 2012b; Mickler et al., 2004; Oster et al., 2012). The BL3 record displays a strong correlation between $\delta^{18}O_c$ and $\delta^{13}C_c$ (R^2 values $\geq$ 0.9) that can reflect out-of-equilibrium precipitation. Trace element incorporation (e.g., Sr) in the carbonate matrix is related to hydroclimate changes and higher Sr/Ca values are commonly interpreted to reflect prior carbonate precipitation - PCP (Baker et al., 1997; Fairchild et al., 2000; Fairchild and Treble, 2009; Frisia et al., 2011; Wassenburg et al., 2020). PCP can be defined as carbonate

precipitation upstream of the final drip site, either in the epikarst or in the cave itself, during i) periods of lower cave pCO_2 prompting CO_2 degassing and precipitation of carbonate or ii) drier periods when an increased proportion of air in the lower epikarst and/or longer residence time of the water on the cave ceiling/stalactites allow CO_2 degassing and precipitation along the flow path. During PCP, many trace elements including Sr preferentially remain in the solution (Morse and Bender, 1990),

480 appearing enriched over Ca in the subsequent carbonate precipitating on the stalagmite. PCP also changes both $\delta^{13}C_c$ and $\delta^{18}O_c$ towards higher values as light isotopes will be removed from the dissolved inorganic carbon (DIC) reservoir during CO_2 degassing (Deininger et al., 2021; Dreybrodt, 2008; Hansen et al., 2019), with increases of up to 2 ‰ and 7 ‰, respectively, for $\delta^{18}O_c$ and $\delta^{13}C_c$ at T=20°C (Hansen et al., 2019). From our dataset we observe a slope of 2.45 for the $\delta^{13}C_c$ vs $\delta^{18}O_c$ correlation which points to incomplete O-isotope buffering between the DIC and H_2O reservoir, based on the Rayleigh

485 distillation model developed by Mickler et al. (2006). In this model, a vertical slope corresponds to complete buffering, while a slope of 0.52 is the theoretical limit for a system with no buffering. The rate of recharge, illustrated by the drip-rate, and cave pCO_2 are considered to be the primary controls on PCP (Fohlmeister et al., 2020; Oster et al., 2012), with both lower cave pCO_2 and lower drip rate favoring PCP either in the lower epikarst or at the cave ceiling (Frisia et al., 2011). Individually, Sr/Ca ratios, $\delta^{18}O_c$ and $\delta^{13}C_c$ can be influenced by a variety of mechanisms (e.g. Fairchild et al., 2000; Fohlmeister et al., 2020;

490 Lachniet, 2009), however the correlation of the three proxies and the fact that the relative amplitude among peaks in both $\delta^{18}O_c$ and $\delta^{13}C_c$ is similar indicates that these proxies are influenced by a common mechanism. We hence propose that stable isotope and Sr/Ca ratios in stalagmite BL3 are controlled primarily by PCP.

Major growth direction changes and dark layers are concomitant with each peak and further examination of these layers reveals signs of dissolution/erosion on top of organic-rich layers. These observations could point to microbial activity during periods

495 of lower drip rate, allowing bacterial communities to colonize the stalagmite surface (pers. Comm. Silvia Frisia). The layers therefore appear to correspond to short hiatuses, indicating that drip water availability rather than ventilation drives PCP in Bloukrantz cave. A likely scenario is therefore that periodic drying episodes caused both the observed variations in the geochemical parameters and the visual changes in the speleothem. As conditions became drier, the drip-rate would have decreased, allowing for more PCP as for example during the period with lower rH in 2018 when there was no active dripping

500 in the cave (Fig. S2). Eventually, calcite growth would stop, allowing for dust to settle at the top (i.e. dark layers) and alteration of stalagmite surfaces, until growth resumed (with or without growth direction change) under wetter conditions.

In addition to the pronounced peaks, both the Sr/Ca ratio and the isotope profiles display an increase in the baseline after ~46 ka that indicates general drying if the same interpretation is applied (i.e. higher values reflect drier conditions). Interestingly, this increase in the baseline at ~46 ka corresponds to a thinning of the stalagmite's width (see Fig. 2) likely due to slower drip-

505 rate as conditions became drier (Fairchild and Baker, 2012a). Overall, the record from 48.3-45.2 ka can thus be interpreted as variable precipitation from 48.3 to 45.2 ka with short, marked drier episodes and overall drying after ~46 ka. Based on our age model, the duration of the dry phases was ~ 200 ± 200 yrs, with relatively large uncertainty due to the 0.3 – 0.8 % uncertainty of the U-Th dates. We also note that the duration of the isotopic peaks could have been even shorter if unresolved hiatuses are

present. Despite the remaining uncertainty in the duration of the dry phases, it is clear that they represent processes operating on sub-millennial (centennial or decadal) timescales.

Comparison with other paleoclimate records is hampered by the scarcity of regional high-resolution records and by the relative short time period covered by our data (<3 kyrs). That being said, the Antarctic temperature record based on $\delta^{18}O$ from the EPICA Dronning Maud Land (EDML) ice core (Epica Community Members et al., 2006; Epica Community Members et al., 2010) shows some similarities. Notably, a cooling phase starting at ~45.9 ka at EDML appears to coincide with what we interpret as overall drying at Bloukrantz cave (Fig. 5). Cooling in Antarctica has been associated with an equatorward shift of the southern westerlies belt, causing a northward extension of the winter rainfall zone along the west coast of Africa (Chase and Meadows, 2007; Engelbrecht et al., 2019; Stuut et al., 2002). This is illustrated in core MD96-2094 from Walvis Ridge off southwest Africa (19°59.97'S, 9°15.87'E), where the Aridity index developed by Stuut et al. (2002) starts decreasing around 46 ka and until 40 ka, matching a speleothem growth period in northern Namibia (18°15.42'S, 13°53.68'E; Railsback et al., 2016), and indicating increased rainfall due to northward movement of the westerlies. Similarly, off Southeast Africa, on the Agulhas Plateau, an increase in ice-rafted debris at ~ 46.1 ka and a gradual decrease in Agulhas Leakage Fauna both in the Cape Basin record (Peeters et al., 2004) and in core CD 154 17-17K (Simon et al., 2013) are associated with a northward shift of the Subtropical Front. These observations have been interpreted as a northward shift of both atmospheric (southern westerlies belt) and oceanic (subtropical front) circulation systems as a result of cooling in Antarctica. On land, a speleothem record from Wolkberg cave, in the Limpopo Province in the northeastern part of South Africa (Holzkämper et al., 2009), spanning the period of ~59 to 46 ka, displays a hiatus at 46.3 ka, coinciding with the onset of overall drier conditions at Bloukrantz cave. The presence of hiatus(es) is generally not systematically linked to drier conditions, however, other records offer some line of evidence for lower precipitations in the summer rainfall zone. The speleothem record from Lobatse cave in Botswana (Holmgren et al., 1995) presents a sharp increase (~6 ‰) in $\delta^{13}C_c$ at ~46 ka followed by constant high $\delta^{13}C_c$ values and a hiatus at 43.2 ka. This signal was interpreted as drier conditions in the northeastern part of South Africa (in the SRZ). Further away, in southwestern Madagascar (24°06'S, 43°46'E) a speleothem growth period from ~48 to 46 ka has been linked to Antarctic isotope maxima (i.e. warmer periods) and high solar summer irradiation, allowing the southward expansion of the intertropical convergence zone and associated rain-bearing system to reach southwestern Madagascar (Burns et al., 2022). The growth period of these records collectively points to overall drier conditions in the Summer rainfall zone between 46 to 43 ka and correlates well with reconstructed rainfall amount at Tswaing crater (Partridge et al., 1997) that shows a decrease in rainfall amount starting at 50 ka and reaching a minimum at 44 ka.

In combination with these lines of evidence from the SRZ, the overall drier conditions at Bloukrantz cave at 46 ka and the subsequent stop in growth at 45.3 ka could be explained by reduced summer rainfall through a northward shift of the southern westerlies belt. Such northward expansion of the WRZ has also been simulated for Last Glacial Maximum conditions (Engelbrecht et al 2019). In the simulation, this northward shift of the westerlies was paired with drier conditions along a narrow stretch along the south coast due to berg-wind conditions along the Cape Fold mountains. Our data indeed suggest that

with Antarctic cooling during MIS 3, winter rainfall did not provide sufficient moisture to sustain carbonate growth at Bloukrantz cave and that the northward expansion of the WRZ is not matched by a similar eastward expansion and/or is linked to reduced westerlies intensity.

In contrast to the overall drying trend, the repeated apparent drying we observe in our record in the form of peaks in isotope ratios and Sr/Ca is not directly matched in the isotopic records from Lobatse cave or Wolkberg cave. However, the Wolkberg record displays some marked variability in aragonite/calcite content with shifts from 100% calcite to >90% aragonite on sub-millennial to millennial timescales (Holzkämper et al., 2009). Holzkämper et al. (2009) tentatively linked higher aragonite content to drier conditions as factors controlling the formation of aragonite are low drip rates, higher temperature and high Mg concentration in the drip water, the latter likely linked to decreased precipitation and longer residence time in the epikarst (Frisia et al., 2002). This could suggest that these sub-millennial events are not restricted to the southern Cape coastal area but may have been more regional.

4.1 Temperature

The good agreement between the youngest (Holocene) microthermometry estimate with measured cave temperature (green diamond in Fig. 3c) shows that the microthermometry method can provide reliable cave temperatures for Bloukrantz cave, despite the challenges posed by the small size of the fluid inclusions in BL3 and scarcity of monophase liquid inclusions. Microthermometry temperatures during the MIS 3 section of our record reveal an average temperature of 18.8 ± 0.5 °C, i.e., about 1 °C warmer compared to present day (Fig. 3c). The slightly warmer temperature is noteworthy given that the time period covered by the record is within the last glacial period, with colder-than-Holocene temperatures in most parts of the world. Our results suggest that, in the southern Cape region of South Africa, the overall globally cooler conditions are offset by other influences, such as changes in ocean circulation or the coastline distance due to lower relative sea level. Offshore of southern Africa, reconstructed SST for MIS 3 are > 1-4 °C colder than modern day in the Indian (Fig. S10; Simon et al. 2013), Southern (Dyez et al. 2014) and Atlantic (Kirst et al., 1999) sectors. The Southern sector (Dyez et al., 2014) records the smallest temperature offset, with 1.0°C colder temperature for MIS 3 than for modern-day, compared to 2.8°C and 4.1°C in the Indian Ocean and Atlantic Ocean respectively. Moreover, a 70 m lower relative sea level during the interval covered by our record (Grant et al., 2012) would have shifted the coastline seawards by almost 10 km (Jacobs et al., 2020). Göktürk et al. (2023) simulated that such a coastline shift would result in drier conditions and more pronounced continentality along the coastline of the southern Cape region, with higher (lower) daily max (min) temperature and overall higher mean annual temperature which could explain why higher than today temperatures are recorded at Bloukrantz cave.

Interestingly, no significant changes in temperature are found during most of the Sr/Ca and isotope peaks, suggesting that the process(es) influencing the calcite composition are not related to temperature. The peaks observed in the calcite-based proxies are also not apparent in the FIWI signal. When PCP occurs, δ^{18}O and δ^{13}C of the DIC increase as primary calcite is precipitated; the δ^{18}O of the DIC will then gradually decrease due to re-equilibration with the water over time (Deininger et al., 2021;

Hansen et al., 2019). If the time between PCP and the subsequent calcite precipitation on the stalagmite is not long enough to allow for O-isotope equilibration with H_2O, $\delta^{18}O_c$ of the stalagmite calcite will be elevated compared to what would be expected from the $\delta^{18}O_w$ and the cave temperature (Deininger et al., 2021; Dreybrodt and Fohlmeister, 2022; Hansen et al.,

640 2019). Indeed, while FIWI temperatures calculated using the T-α relationship from Tremaine et al. (2011) show generally very good agreement with microthermometry from 48.3 to 45.8 ka, they deviate during the isotopic peaks with FIWI-T ~3°C colder than the corresponding microthermometry. The FIWI results thus further support our interpretation of the isotope peaks as cave-internal processes controlled by hydroclimate.

After 46 ka, FIWI temperatures clearly depart from microthermometry estimates with values 5 to 15°C warmer. In $\delta^{18}O_w$ vs

645 $\delta^{2}H_w$ space, these younger samples plot as a distinct cluster away from the LMWL, in contrast to the samples older than ~46 ka (Fig. 4). Such departure from the LMWL has been observed in other studies (Van Breukelen et al., 2008; Wainer et al., 2011; Warken et al., 2022) and could point either to analytical artefacts (e.g. Fernandez et al., 2023; Matthews et al., 2021) or to in-cave processes such as evaporation (Warken et al., 2022). Water content in the samples can in some cases track potential water loss during the analytical procedure as fabric amenable to leaking will result in both lower water content and a departure

650 from the MWL (Fernandez et al., 2023; Matthews et al., 2021). Here, the water content displays little variation through most of the record (Fig. 4 and Fig. S7) except for 2 samples with higher water content at ~45.9 ka, just before the FIWI data depart from the LMWL. In addition, replicate measurements of the younger samples do not show any trend in $\delta^{18}O_w$ vs $\delta^{2}H_w$ space as would be expected from variable partial loss of water during heating of the samples (Fernandez et al., 2023). Further, no changes in the speleothem fabric were detected that could explain a change in behavior during analysis for these samples. We

655 thus do not have any evidence that suggests analytical artefacts could cause the departure of the younger MIS 3 samples away from the LMWL.

An alternative explanation could be in-cave evaporation (e.g. Warken et al., 2022). Using a Craig-Gordon evaporation model (Craig and Gordon, 1965) with an n value of 1 (i.e. non-turbulent atmosphere), and the average $\delta^{2}H_w$ and $\delta^{18}O_w$ values from the data points > 46 ka as a starting point, <5% loss to evaporation under rH between 80 to 85 % could explain the isotopic

660 values of the younger samples. These are not unrealistic conditions, as rH of 86 % has been measured when no dripping was observed in the cave (Fig. S2). Cave evaporation occurs when relative humidity decreases as a consequence of i) better ventilation, when the cave air is partially replaced by outside air with a lower rH, or ii) lower drip rate, decreasing the water supply to the cave and thus the rH. Wind-induced changes in ventilation seem unlikely given the cave geometry, whereas changes in ventilation induced by thermal convection (Fairchild and Baker, 2012c) are not supported by the apparently constant

665 microthermometry temperatures during most of the record. We hence suggest that slower drip rate and lower water supply could be the cause for lower rH, leading to evaporation in the cave and elevated $\delta^{18}O_w$ and $\delta^{2}H_w$ of the younger samples at the end of the MIS 3 section. This interpretation is also in line with the calcite-based proxies suggesting a drying trend leading up to the prominent growth hiatus.

5 Summary and conclusions

This study presents a 3 kyr long, high-resolution and multi-proxy record of temperature and hydroclimate at the southern coast of South Africa during MIS 3 (45.2-48.3 ka). Based on fluid inclusion microthermometry, we reconstruct an average cave temperature for the MIS 3 section of the stalagmite of 18.8 ± 0.5 °C, slightly warmer compared to the present day. This difference could be due to increased continentality. We find generally good agreement between the microthermometry and water isotope-based temperature estimates, with exceptions during parts of the record where other proxies indicate drier conditions.

During the investigated time interval of MIS 3, precipitation at the site appears to have been highly variable. Short episodes of higher $\delta^{18}O_c$, $\delta^{13}C_c$ and Sr/Ca values are likely linked to Prior Carbonate Precipitation and to drier conditions. These fluctuations in hydroclimate do not appear to be accompanied by substantial changes in temperature.

After 46 ka, a trend in the calcite proxy baselines and a distinctly different isotope signal in the fluid inclusions is interpreted to reflect overall drier conditions with potential evaporation in the cave. Drier conditions between 46 to 43 ka are also observed in other records from the Summer Rainfall Zone, whereas wetter conditions were reconstructed further north in Namibia. Given a coeval cooling at Dronning Maud Land in Antarctica, these observations together suggest a potential influence of the Antarctic ice sheet through a northward displacement of the Southern westerly wind belt shifting the rain pattern over South Africa.

Data availability

All results from this study are available in the appendix to this publication.

Author Contribution

Study design: JM, ANM, SEL; Methodology and data-acquisition: JM, TB, HAR, AFB, YK, JA, SA, ML; Visualization and original draft preparation: JM; Writing and editing: JM, ANM, SEL, TB, HAR, AFB, YK, JA, SA, ML.

Competing interest

The authors declare that they have no conflict of interest.

Acknowledgements

This work was funded by the Research Council of Norway through its Centres of Excellence funding scheme, SFF Centre for Early Sapiens Behaviour (SapienCE), project number 262618. Analyses were enabled by access to the national analytical

---

4.3 Significance for the archeological record¶
MIS 3 archeological sites display an undeniable change from the previous Howieson's Poort technological complex, with for instance fewer ornaments or decorated items (Cochrane, 2008; Mitchell, 2008; Wadley, 2015 and references therein). This change is also marked by a geographical shift from modern coastal (e.g. Blombos cave) to more inland sites (e.g. Sibudu, Rose Cottage, Melikane). Moreover, local variability in lithic assemblages during MIS 3 has been inferred to reflect fewer interactions between different groups/populations possibly driven by MIS 3 environmental uncertainty (Mackay et al., 2014). However, the short time period covered by our record prevents any environmental-based conclusions and highlights the need for longer high-resolution paleoclimate reconstructions in the region.¶

infrastructure at UiB at Farlab (NFR grant number 245907) and EARTHLAB (NFR grant number 226171/F50); at the University of Bern the analytical work was funded by SNF grant numbers SNF-132646 (Stalclim), SNF-147674 (Stalclim II) and SNF-159563. A.F. acknowledges support from Juan de la Cierva Fellowship (IJC2019040065-I) granted by the Spanish Ministry of Science and Innovation and co-funded by the European Development Fund and the European Social Fund. We thank the South African Heritage Resources Agency (SAHRA), Heritage Western Cape (HWC) and Cape Nature for granting the permits to enter the De Hoop Nature Reserve and collect speleothem samples for scientific analysis. We thank Ole Fredrik Unhammer, Magnus Mathisen Haaland, Sverre Asknes and Prof. Simon Armitage for their help with fieldwork. Samantha Mienies at Wits University is thanked for curating the samples and helping with the permits. We thank Prof. Silvia Frisia at University of Newcastle for her help with the petrographic observations. Prof. Harald Sodemann at UiB is thanked for his advice on the micro drop system. We thank Prof. Hai Cheng and Xuexue Jia for supplementary U-Th dating performed during Covid-19 lockdown. We also thank Dr. Steffen Holzkämper, Prof. Karen Holmgren, Dr. Margit Simon, Dr. Brian Chase and Dr. Kerstin Braun for respectively providing the Wolkberg cave speleothem data, the Lobatse cave speleothem data, the Tswaing crater data, the Cape Basin marine record and the Cango cave data. We thank both Dr. Kerstin Braun and Dr. Nick Scroxton for their thorough and constructive reviews.

References

Adigun, J.: Investigating the archaeological implications of environmental change during the Middle Stone Age: a contribution from the geochemical analysis of speleothems in the southern Cape, South Africa (https://wiredspace.wits.ac.za/handle/10539/21240), Faculty of Science, University of the Witwatersrand, Johannesburg, 2016.

Affek, H. P., Bar-Matthews, M., Ayalon, A., Matthews, A., and Eiler, J. M.: Glacial/interglacial temperature variations in Soreq cave speleothems as recorded by 'clumped isotope' thermometry, Geochimica et Cosmochimica Acta, 72, 5351-5360, https://doi.org/10.1016/j.gca.2008.06.031, 2008.

Affolter, S., Fleitmann, D., and Leuenberger, M.: New online method for water isotope analysis of speleothem fluid inclusions using laser absorption spectroscopy (WS-CRDS), Climate of the Past, 10, 1291-1304, 10.5194/cp-10-1291-2014, 2014.

Affolter, S., Häuselmann, A., Fleitmann, D., Edwards, R. L., Cheng, H., and Leuenberger, M.: Central Europe temperature constrained by speleothem fluid inclusion water isotopes over the past 14,000 years, Science Advances, 5, eaav3809, 10.1126/sciadv.aav3809, 2019.

Andersen, K. K., Azuma, N., Barnola, J. M., Bigler, M., Biscaye, P., Caillon, N., Chappellaz, J., Clausen, H. B., Dahl-Jensen, D., Fischer, H., Flückiger, J., Fritzsche, D., Fujii, Y., Goto-Azuma, K., Grønvold, K., Gundestrup, N. S., Hansson, M., Huber, C., Hvidberg, C. S., Johnsen, S. J., Jonsell, U., Jouzel, J., Kipfstuhl, S., Landais, A., Leuenberger, M., Lorrain, R., Masson-Delmotte, V., Miller, H., Motoyama, H., Narita, H., Popp, T., Rasmussen, S. O., Raynaud, D., Rothlisberger, R., Ruth, U., Samyn, D., Schwander, J., Shoji, H., Siggard-Andersen, M. L., Steffensen, J. P., Stocker, T., Sveinbjörnsdóttir, A. E.,

770   Svensson, A., Takata, M., Tison, J. L., Thorsteinsson, T., Watanabe, O., Wilhelms, F., White, J. W. C., and North Greenland Ice Core Project, m.: High-resolution record of Northern Hemisphere climate extending into the last interglacial period, Nature, 431, 147-151, 10.1038/nature02805, 2004.

Baker, A., Ito, E., Smart, P. L., and McEwan, R. F.: Elevated and variable values of 13C in speleothems in a British cave system, Chemical Geology, 136, 263-270, https://doi.org/10.1016/S0009-2541(96)00129-5, 1997.

775   Bar-Matthews, M., Marean, C. W., Jacobs, Z., Karkanas, P., Fisher, E. C., Herries, A. I. R., Brown, K., Williams, H. M., Bernatchez, J., Ayalon, A., and Nilssen, P. J.: A high resolution and continuous isotopic speleothem record of paleoclimate and paleoenvironment from 90 to 53 ka from Pinnacle Point on the south coast of South Africa, Quaternary Science Reviews, 29, 2131-2145, 10.1016/j.quascirev.2010.05.009, 2010.

Blyth, A. J. and Schouten, S.: Calibrating the glycerol dialkyl glycerol tetraether temperature signal in speleothems,
780   Geochimica et Cosmochimica Acta, 109, 312-328, https://doi.org/10.1016/j.gca.2013.02.009, 2013.

Braun, K., Bar-Matthews, M., Ayalon, A., Zilberman, T., and Matthews, A.: Rainfall isotopic variability at the intersection between winter and summer rainfall regimes in coastal South Africa (Mossel Bay, Western Cape Province), South African Journal of Geology, 120, 323-340, 10.25131/gssajg.120.3.323, 2017.

Braun, K., Nehme, C., Pickering, R., Rogerson, M., and Scroxton, N.: A Window into Africa's Past Hydroclimates: The
785   SISAL_v1 Database Contribution, 10.3390/quat2010004, 2019a.

Braun, K., Bar-Matthews, M., Matthews, A., Ayalon, A., Cowling, R. M., Karkanas, P., Fisher, E. C., Dyez, K., Zilberman, T., and Marean, C. W.: Late Pleistocene records of speleothem stable isotopic compositions from Pinnacle Point on the South African south coast, Quaternary Research, 91, 265-288, 10.1017/qua.2018.61, 2019b.

Braun, K., Bar-Matthews, M., Matthews, A., Ayalon, A., Zilberman, T., Cowling, R. M., Fisher, E. C., Herries, A. I. R., Brink,
790   J. S., and Marean, C. W.: Comparison of climate and environment on the edge of the Palaeo-Agulhas Plain to the Little Karoo (South Africa) in Marine Isotope Stages 5–3 as indicated by speleothems, Quaternary Science Reviews, 235, 105803, https://doi.org/10.1016/j.quascirev.2019.06.025, 2020.

Burns, S. J., McGee, D., Scroxton, N., Kinsley, C. W., Godfrey, L. R., Faina, P., and Ranivoharimanana, L.: Southern Hemisphere controls on ITCZ variability in southwest Madagascar over the past 117,000 years, Quaternary Science Reviews,
795   276, 107317, https://doi.org/10.1016/j.quascirev.2021.107317, 2022.

Carr, A. S., Thomas, D. S. G., Bateman, M. D., Meadows, M. E., and Chase, B.: Late Quaternary palaeoenvironments of the winter-rainfall zone of southern Africa: Palynological and sedimentological evidence from the Agulhas Plain, Palaeogeography Palaeoclimatology Palaeoecology, 239, 147-165, 10.1016/j.palaeo.2006.01.014, 2006.

Chase, B. M.: South African palaeoenvironments during marine oxygen isotope stage 4: a context for the Howiesons Poort
800   and Still Bay industries, Journal of Archaeological Science, 37, 1359-1366, 10.1016/j.jas.2009.12.040, 2010.

Chase, B. M. and Meadows, M. E.: Late Quaternary dynamics of southern Africa's winter rainfall zone, Earth-Science Reviews, 84, 103-138, 10.1016/j.earscirev.2007.06.002, 2007.

Deleted:

Chase, B., Harris, C., de Wit, M. J., Kramers, J., Doel, S., and Stankiewicz, J.: South African speleothems reveal influence of
805   high- and low-latitude forcing over the past 113.5 k.y, Geology, 49, 1353-1357, 10.1130/G49323.1, 2021.

Cheng, H., Lawrence Edwards, R., Shen, C.-C., Polyak, V. J., Asmerom, Y., Woodhead, J., Hellstrom, J., Wang, Y., Kong,
X., Spötl, C., Wang, X., and Calvin Alexander, E.: Improvements in 230Th dating, 230Th and 234U half-life values, and U–
Th isotopic measurements by multi-collector inductively coupled plasma mass spectrometry, Earth and Planetary Science
Letters, 371-372, 82-91, https://doi.org/10.1016/j.epsl.2013.04.006, 2013.

810   Craig, H. and Gordon, L.: Deuterium and oxygen 18 variations in the ocean and the marine atmosphere, Stable Isotopes in
Oceanographic Studies and Paleotemperatures E, Proceedings of the Third Spoleto Conference, Spoleto, Italy, edited by E.
Tongiori, 9-130,

D'Errico, F.: The invisible frontier. A multiple species model for the origin of behavioral modernity, Evolutionary
Anthropology: Issues, News, and Reviews, 12, 188-202, https://doi.org/10.1002/evan.10113, 2003.

815   de Graaf, S., Vonhof, H. B., Weissbach, T., Wassenburg, J. A., Levy, E. J., Kluge, T., and Haug, G. H.: A comparison of
isotope ratio mass spectrometry and cavity ring-down spectroscopy techniques for isotope analysis of fluid inclusion water,
Rapid Communications in Mass Spectrometry, 34, 10.1002/rcm.8837, 2020.

Deininger, M., Hansen, M., Fohlmeister, J., Schröder-Ritzrau, A., Burstyn, Y., and Scholz, D.: Are oxygen isotope
fractionation factors between calcite and water derived from speleothems systematically biased due to prior calcite
820   precipitation (PCP)?, Geochimica et Cosmochimica Acta, 305, 212-227, https://doi.org/10.1016/j.gca.2021.03.026, 2021.

Dreybrodt, W.: Evolution of the isotopic composition of carbon and oxygen in a calcite precipitating H_2O–CO_2–$CaCO_3$
solution and the related isotopic composition of calcite in stalagmites, Geochimica et Cosmochimica Acta, 72, 4712-4724,
https://doi.org/10.1016/j.gca.2008.07.022, 2008.

Dreybrodt, W. and Fohlmeister, J.: The impact of outgassing of CO_2 and prior calcium precipitation to the isotope composition
825   of calcite precipitated on stalagmites. Implications for reconstructing climate information from proxies, Chemical Geology,
589, 120676, https://doi.org/10.1016/j.chemgeo.2021.120676, 2022.

Dyez, K. A., Zahn, R., and Hall, I. R.: Multicentennial Agulhas leakage variability and links to North Atlantic climate during
the past 80,000 years, Paleoceanography, 29, 1238-1248, https://doi.org/10.1002/2014PA002698, 2014.

Edwards, R. L.: High precision thorium-230 ages of corals and the timing of sea level fluctuations in the late Quaternary
830   (Ph.D.), Ph.D. thesis, California Institute of California, 1988.

Engelbrecht, C. J., Landman, W. A., Engelbrecht, F. A., and Malherbe, J.: A synoptic decomposition of rainfall over the Cape
south coast of South Africa, Climate Dynamics, 44, 2589-2607, 10.1007/s00382-014-2230-5, 2015.

Engelbrecht, F. A., Marean, C. W., Cowling, R. M., Engelbrecht, C. J., Neumann, F. H., Scott, L., Nkoana, R., O'Neal, D.,
Fisher, E., Shook, E., Franklin, J., Thatcher, M., McGregor, J. L., Van der Merwe, J., Dedekind, Z., and Difford, M.:
835   Downscaling Last Glacial Maximum climate over southern Africa, Quaternary Science Reviews, 226, 105879,
https://doi.org/10.1016/j.quascirev.2019.105879, 2019.

Epica Community Members, Barbante, C., Barnola, J. M., Becagli, S., Beer, J., Bigler, M., Boutron, C., Blunier, T., Castellano, E., Cattani, O., Chappellaz, J., Dahl-Jensen, D., Debret, M., Delmonte, B., Dick, D., Falourd, S., Faria, S., Federer, U., Fischer, H., Freitag, J., Frenzel, A., Fritzsche, D., Fundel, F., Gabrielli, P., Gaspari, V., Gersonde, R., Graf, W., Grigoriev, D., Hamann, I., Hansson, M., Hoffmann, G., Hutterli, M. A., Huybrechts, P., Isaksson, E., Johnsen, S., Jouzel, J.,
845 Kaczmarska, M., Karlin, T., Kaufmann, P., Kipfstuhl, S., Kohno, M., Lambert, F., Lambrecht, A., Lambrecht, A., Landais, A., Lawer, G., Leuenberger, M., Littot, G., Loulergue, L., Lüthi, D., Maggi, V., Marino, F., Masson-Delmotte, V., Meyer, H., Miller, H., Mulvaney, R., Narcisi, B., Oerlemans, J., Oerter, H., Parrenin, F., Petit, J. R., Raisbeck, G., Raynaud, D., Röthlisberger, R., Ruth, U., Rybak, O., Severi, M., Schmitt, J., Schwander, J., Siegenthaler, U., Siggaard-Andersen, M. L., Spahni, R., Steffensen, J. P., Stenni, B., Stocker, T. F., Tison, J. L., Traversi, R., Udisti, R., Valero-Delgado, F., van den
850 Broeke, M. R., van de Wal, R. S. W., Wagenbach, D., Wegner, A., Weiler, K., Wilhelms, F., Winther, J. G., and Wolff, E.: One-to-one coupling of glacial climate variability in Greenland and Antarctica, Nature, 444, 195-198, 10.1038/nature05301, 2006.

Epica Community Members, Stable oxygen isotopes of ice core EDML, PANGAEA [dataset], 10.1594/PANGAEA.754444, 2010.

855 Epstein, S., Buchsbaum, R., Lowenstam, H., and Urey, H. C.: Carbonate-Water Istotopic Temperature Scale, Geological Society of America Bulletin, 62, 417-426, 10.1130/0016-7606(1951)62[417:CITS]2.0.CO;2, 1951.

Epstein, S., Buchsbaum, R., Lowenstam, H. A., and Urey, H. C.: Revised Carbonate-Water Isotopic Temperature Scale, Geological Society of America Bulletin, 64, 1315-1325, 10.1130/0016-7606(1953)64[1315:RCITS]2.0.CO;2, 1953.

Fairchild, I. J. and Baker, A.: The Architecture of Speleothems, Speleothem Science, 105-147 pp.,
860 https://doi.org/10.1002/9781444361094.ch4, 2012a.

Fairchild, I. J. and Baker, A.: The Holocene Epoch: Testing the Climate and Environmental Proxies, Speleothem Science, 324-352, https://doi.org/10.1002/9781444361094.ch11, 2012b.

Fairchild, I. J. and Baker, A.: The Speleothem Incubator, Speleothem Science, 105-147 pp., https://doi.org/10.1002/9781444361094.ch4, 2012c.

865 Fairchild, I. J. and Treble, P. C.: Trace elements in speleothems as recorders of environmental change, Quaternary Science Reviews, 28, 449-468, https://doi.org/10.1016/j.quascirev.2008.11.007, 2009.

Fairchild, I. J., Borsato, A., Tooth, A. F., Frisia, S., Hawkesworth, C. J., Huang, Y., McDermott, F., and Spiro, B.: Controls on trace element (Sr–Mg) compositions of carbonate cave waters: implications for speleothem climatic records, Chemical Geology, 166, 255-269, https://doi.org/10.1016/S0009-2541(99)00216-8, 2000.

870 Fernandez, A., Løland, M. H., Maccali, J., Krüger, Y., Vonhof, H. B., Sodemann, H., and Meckler, A. N.: Characterisation and correction of evaporative artifacts in speleothem fluid inclusion isotope analysis as applied to a stalagmite from Borneo, 24, e2023GC010857, https://doi.org/10.1029/2023GC010857, 2023.

Deleted: ESS Open Archive, https://doi.org/10.22541/essoar.167340715.57808428/v1, 2020, 2023.

Fohlmeister, J., Voarintsoa, N. R. G., Lechleitner, F. A., Boyd, M., Brandtstätter, S., Jacobson, M. J., and L. Oster, J.: Main controls on the stable carbon isotope composition of speleothems, Geochimica et Cosmochimica Acta, 279, 67-87, https://doi.org/10.1016/j.gca.2020.03.042, 2020.

Frisia, S.: Microstratigraphic logging of calcite fabrics in speleothems as tool for palaeoclimate studies, International Journal of Speleology, 44, 1-16, 10.5038/1827-806X.44.1.1, 2015.

Frisia, S., Borsato, A., Fairchild, I. J., McDermott, F., and Selmo, E. M.: Aragonite-calcite relationships in speleothems (Grotte de Clamouse, France): Environment, fabrics, and carbonate geochemistry, Journal of Sedimentary Research, 72, 687-699, 10.1306/020702720687, 2002.

Frisia, S., Fairchild, I. J., Fohlmeister, J., Miorandi, R., Spötl, C., and Borsato, A.: Carbon mass-balance modelling and carbon isotope exchange processes in dynamic caves, Geochimica et Cosmochimica Acta, 75, 380-400, https://doi.org/10.1016/j.gca.2010.10.021, 2011.

Göktürk, O. M., Sobolowski, S. P., Simon, M. H., Zhang, Z., and Jansen, E.: Sensitivity of coastal southern African climate to changes in coastline position and associated land extent over the last glacial, Quaternary Science Reviews, 300, 107893, https://doi.org/10.1016/j.quascirev.2022.107893, 2023.

Grant, K. M., Rohling, E. J., Bar-Matthews, M., Ayalon, A., Medina-Elizalde, M., Ramsey, C. B., Satow, C., and Roberts, A. P.: Rapid coupling between ice volume and polar temperature over the past 150,000 years, Nature, 491, 744-747, 10.1038/nature11593, 2012.

Hansen, M., Scholz, D., Schöne, B. R., and Spötl, C.: Simulating speleothem growth in the laboratory: Determination of the stable isotope fractionation (δ^{13}C and δ^{18}O) between H2O, DIC and CaCO3, Chemical Geology, 509, 20-44, https://doi.org/10.1016/j.chemgeo.2018.12.012, 2019.

Henshilwood, C. S., D'Errico, F., Van Niekerk, K. L., Coquinot, Y., Jacobs, Z., Lauritzen, S. E., Menu, M., and García-Moreno, R.: A 100,000-year-old ochre-processing workshop at Blombos Cave, South Africa, Science, 334, 219-222, 10.1126/science.1211535, 2011.

Henshilwood, C. S., van Niekerk, K. L., Wurz, S., Delagnes, A., Armitage, S. J., Rifkin, R. F., Douze, K., Keene, P., Haaland, M. M., Reynard, J., Discamps, E., and Mienies, S. S.: Klipdrift Shelter, southern Cape, South Africa: preliminary report on the Howiesons Poort layers, Journal of Archaeological Science, 45, 284-303, https://doi.org/10.1016/j.jas.2014.01.033, 2014.

Holmgren, K., Karlén, W., and Shaw, P. A.: Paleoclimatic Significance of the Stable Isotopic Composition and Petrology of a Late Pleistocene Stalagmite from Botswana, Quaternary Research, 43, 320-328, 10.1006/qres.1995.1038, 1995.

Holzkämper, S., Holmgren, K., Lee-Thorp, J., Talma, S., Mangini, A., and Partridge, T.: Late Pleistocene stalagmite growth in Wolkberg Cave, South Africa, Earth and Planetary Science Letters, 282, 212-221, https://doi.org/10.1016/j.epsl.2009.03.016, 2009.

Huber, C., Leuenberger, M., Spahni, R., Flückiger, J., Schwander, J., Stocker, T. F., Johnsen, S., Landais, A., and Jouzel, J.: Isotope calibrated Greenland temperature record over Marine Isotope Stage 3 and its relation to CH4, Earth and Planetary Science Letters, 243, 504-519, https://doi.org/10.1016/j.epsl.2006.01.002, 2006.

Jacobs, Z., Jones, B. G., Cawthra, H. C., Henshilwood, C. S., and Roberts, R. G.: The chronological, sedimentary and environmental context for the archaeological deposits at Blombos Cave, South Africa, Quaternary Science Reviews, 235, 105850, https://doi.org/10.1016/j.quascirev.2019.07.032, 2020.

920   Kindler, P., Guillevic, M., Baumgartner, M., Schwander, J., Landais, A., and Leuenberger, M.: Temperature reconstruction from 10 to 120 kyr b2k from the NGRIP ice core, Clim. Past, 10, 887-902, 10.5194/cp-10-887-2014, 2014.

Kirst, G. J., Schneider, R. R., Müller, P. J., von Storch, I., and Wefer, G.: Late Quaternary Temperature Variability in the Benguela Current System Derived from Alkenones, Quaternary Research, 52, 92-103, 10.1006/qres.1999.2040, 1999.

Kluge, T., Marx, T., Scholz, D., Niggemann, S., Mangini, A., and Aeschbach-Hertig, W.: A new tool for palaeoclimate reconstruction: Noble gas temperatures from fluid inclusions in speleothems, Earth and Planetary Science Letters, 269, 408-

925   415, https://doi.org/10.1016/j.epsl.2008.02.030, 2008.

Krüger, Y., Marti, D., Staub, R. H., Fleitmann, D., and Frenz, M.: Liquid-vapour homogenisation of fluid inclusions in stalagmites: Evaluation of a new thermometer for palaeoclimate research, Chemical Geology, 289, 39-47, 10.1016/j.chemgeo.2011.07.009, 2011.

Lachniet, M. S.: Climatic and environmental controls on speleothem oxygen-isotope values, Quaternary Science Reviews, 28,

930   412-432, https://doi.org/10.1016/j.quascirev.2008.10.021, 2009.

Løland, M. H., Krüger, Y., Fernandez, A., Buckingham, F., Carolin, S. A., Sodemann, H., Adkins, J. F., Cobb, K. M., and Meckler, A. N.: Evolution of tropical land temperature across the last glacial termination, Nature Communications, 13, 5158, 10.1038/s41467-022-32712-3, 2022.

Ludwig, K. R.: User's Manual for Isoplot 3.00: A Geochronological Toolkit for Microsoft Excel, Berkeley Geochronology

935   Center Special publication, 4, 2003.

Marean, C. W., Bar-Matthews, M., Bernatchez, J., Fisher, E., Goldberg, P., Herries, A. I. R., Jacobs, Z., Jerardino, A., Karkanas, P., Minichillo, T., Nilssen, P. J., Thompson, E., Watts, I., and Williams, H. M.: Early human use of marine resources and pigment in South Africa during the Middle Pleistocene, Nature, 449, 905-908, 10.1038/nature06204, 2007.

Marti, D., Kruger, Y., Fleitmann, D., Frenz, M., and Ricka, J.: The effect of surface tension on liquid-gas equilibria in isochoric

940   systems and its application to fluid inclusions, Fluid Phase Equilibria, 314, 13-21, 10.1016/j.fluid.2011.08.010, 2012.

Matthews, A., Affek, H. P., Ayalon, A., Vonhof, H. B., and Bar-Matthews, M.: Eastern Mediterranean climate change deduced from the Soreq Cave fluid inclusion stable isotopes and carbonate clumped isotopes record of the last 160 ka, Quaternary Science Reviews, 272, 10.1016/j.quascirev.2021.107223, 2021.

McCrea, J. M.: On the Isotopic Chemistry of Carbonates and a Paleotemperature Scale, Journal of Chemical Physics, 18, 849-

945   857, 10.1063/1.1747785, 1950.

Meckler, A. N., Affolter, S., Dublyansky, Y. V., Krüger, Y., Vogel, N., Bernasconi, S. M., Frenz, M., Kipfer, R., Leuenberger, M., Spötl, C., Carolin, S., Cobb, K. M., Moerman, J., Adkins, J. F., and Fleitmann, D.: Glacial-interglacial temperature change in the tropical West Pacific: A comparison of stalagmite-based paleo-thermometers, Quaternary Science Reviews, 127, 90-116, 10.1016/j.quascirev.2015.06.015, 2015.

Mickler, P. J., Stern, L. A., and Banner, J. L.: Large kinetic isotope effects in modern speleothems, GSA Bulletin, 118, 65-81, 10.1130/B25698.1, 2006.

Mickler, P. J., Banner, J. L., Stern, L., Asmerom, Y., Edwards, R. L., and Ito, E.: Stable isotope variations in modern tropical speleothems: Evaluating equilibrium vs. kinetic isotope effects 1 1Associate editor: E. M. Ripley, Geochimica et Cosmochimica Acta, 68, 4381-4393, https://doi.org/10.1016/j.gca.2004.02.012, 2004.

Morse, J. W. and Bender, M. L.: Partition coefficients in calcite: Examination of factors influencing the validity of experimental results and their application to natural systems, Chemical Geology, 82, 265-277, https://doi.org/10.1016/0009-2541(90)90085-L, 1990.

Noah, J.: Reconstructing palaeoenvironments during the Middle Stone Age in the southern Cape, South Africa: stable isotope analysis of speleothems from the De Hoop Nature Reserve, Faculty of Science, University of the Wiwatersrand, Johannesburg, 2011.

Oster, J. L., Montañez, I. P., and Kelley, N. P.: Response of a modern cave system to large seasonal precipitation variability, Geochimica et Cosmochimica Acta, 91, 92-108, https://doi.org/10.1016/j.gca.2012.05.027, 2012.

Partridge, T. C., Demenocal, P. B., Lorentz, S. A., Paiker, M. J., and Vogel, J. C.: Orbital forcing of climate over South Africa: A 200,000-year rainfall record from the pretoria saltpan, Quaternary Science Reviews, 16, 1125-1133, https://doi.org/10.1016/S0277-3791(97)00005-X, 1997.

Peeters, F. J. C., Acheson, R., Brummer, G.-J. A., de Ruijter, W. P. M., Schneider, R. R., Ganssen, G. M., Ufkes, E., and Kroon, D.: Vigorous exchange between the Indian and Atlantic oceans at the end of the past five glacial periods, Nature, 430, 661-665, 10.1038/nature02785, 2004.

Poulson, T. L. and White, W. B.: Cave Environment, Science, 165, 971-+, 1969.

Quick, L. J., Meadows, M. E., Bateman, M. D., Kirsten, K. L., Mäusbacher, R., Haberzettl, T., and Chase, B. M.: Vegetation and climate dynamics during the last glacial period in the fynbos-afrotemperate forest ecotone, southern Cape, South Africa, Quaternary International, 404, 136-149, https://doi.org/10.1016/j.quaint.2015.08.027, 2016.

Railsback, L. B., Brook, G. A., Liang, F., Marais, E., Cheng, H., and Edwards, R. L.: A multi-proxy stalagmite record from northwestern Namibia of regional drying with increasing global-scale warmth over the last 47kyr: The interplay of a globally shifting ITCZ with regional currents, winds, and rainfall, Palaeogeography, Palaeoclimatology, Palaeoecology, 461, 109-121, https://doi.org/10.1016/j.palaeo.2016.08.014, 2016.

Roffe, S. J., Fitchett, J. M., and Curtis, C. J.: Classifying and mapping rainfall seasonality in South Africa: a review, South African Geographical Journal, 101, 158-174, 10.1080/03736245.2019.1573151, 2019.

Rokkan, H. A.: Sporelementer i speleothemer - klimasignal og markørhorisonter (https://bora.uib.no/bora-xmlui/handle/1956/20933), Department of Earth sciences, University of Bergen, 2019.

Scholz, D. and Hoffmann, D. L.: StalAge – An algorithm designed for construction of speleothem age models, Quaternary Geochronology, 6, 369-382, https://doi.org/10.1016/j.quageo.2011.02.002, 2011.

Scroxton, N., Burns, S., Dawson, P., Rhodes, J. M., Brent, K., McGee, D., Heijnis, H., Gadd, P., Hantoro, W., and Gagan, M.:
995   Rapid measurement of strontium in speleothems using core-scanning micro X-ray fluorescence, Chemical Geology, 487, 12-22, https://doi.org/10.1016/j.chemgeo.2018.04.008, 2018.

Siddall, M., Rohling, E. J., Thompson, W. G., and Waelbroeck, C.: Marine isotope stage 3 sea level fluctuations: Data synthesis and new outlook, Reviews of Geophysics, 46, https://doi.org/10.1029/2007RG000226, 2008.

Simon, M. H., Arthur, K. L., Hall, I. R., Peeters, F. J. C., Loveday, B. R., Barker, S., Ziegler, M., and Zahn, R.: Millennial-
1000   scale Agulhas Current variability and its implications for salt-leakage through the Indian–Atlantic Ocean Gateway, Earth and Planetary Science Letters, 383, 101-112, https://doi.org/10.1016/j.epsl.2013.09.035, 2013.

Sodemann, H., Dekhtyareva, A., Fernandez, A., Seidl, A., and Maccali, J.: A flexible device to produce a gas stream with precisely controlled water vapour mixing ratio and isotope composition based on microdrop dispensing technology, Atmos. Meas. Tech. Discuss., 2023, 1-33, , https://doi.org/10.5194/amt-2023-55, 2023.

1005   Stoll, H. M., Müller, W., and Prieto, M.: I-STAL, a model for interpretation of Mg/Ca, Sr/Ca and Ba/Ca variations in speleothems and its forward and inverse application on seasonal to millennial scales, Geochemistry, Geophysics, Geosystems, 13, https://doi.org/10.1029/2012GC004183, 2012.

Strobel, P., Bliedtner, M., Carr, A. S., Struck, J., du Plessis, N., Glaser, B., Meadows, M. E., Quick, L. J., Zech, M., Zech, R., and Haberzettl, T.: Reconstructing Late Quaternary precipitation and its source on the southern Cape coast of South Africa:
1010   A multi-proxy paleoenvironmental record from Vankervelsvlei, Quaternary Science Reviews, 284, 107467, https://doi.org/10.1016/j.quascirev.2022.107467, 2022.

Stuut, J.-B. W., Prins, M. A., Schneider, R. R., Weltje, G. J., Jansen, J. H. F., and Postma, G.: A 300-kyr record of aridity and wind strength in southwestern Africa: inferences from grain-size distributions of sediments on Walvis Ridge, SE Atlantic, Marine Geology, 180, 221-233, https://doi.org/10.1016/S0025-3227(01)00215-8, 2002.

1015   Talma, A. S. and Vogel, J. C.: Late Quaternary Paleotemperatures Derived from a Speleothem from Cango Caves, Cape Province, South Africa, Quaternary Research, 37, 203-213, 10.1016/0033-5894(92)90082-T, 1992.

Taylor, S. R. and McLennan, S. M.: The Continental Crust: its Composition and Evolution, Geoscience Texts, Blackwell Scientific Publications, Oxford, 312 pp.1985.

Tremaine, D. M., Froelich, P. N., and Wang, Y.: Speleothem calcite farmed in situ: Modern calibration of δ18O and δ13C
1020   paleoclimate proxies in a continuously-monitored natural cave system, Geochimica et Cosmochimica Acta, 75, 4929-4950, https://doi.org/10.1016/j.gca.2011.06.005, 2011.

Urey, H. C.: The Thermodynamic Properties of Isotopic Substances, Journal of the Chemical Society, 562-581, 10.1039/jr9470000562, 1947.

van Breukelen, M. R., Vonhof, H. B., Hellstrom, J. C., Wester, W. C. G., and Kroon, D.: Fossil dripwater in stalagmites reveals
1025   Holocene temperature and rainfall variation in Amazonia, Earth and Planetary Science Letters, 275, 54-60, https://doi.org/10.1016/j.epsl.2008.07.060, 2008.

Van Meerbeeck, C. J., Renssen, H., and Roche, D. M.: How did Marine Isotope Stage 3 and Last Glacial Maximum climates differ? - Perspectives from equilibrium simulations, Climate of the past, 5, 33-51, 10.5194/cp-5-33-2009, 2009.

Vonhof, H. B., van Breukelen, M. R., Postma, O., Rowe, P. J., Atkinson, T. C., and Kroon, D.: A continuous-flow crushing device for on-line delta H-2 analysis of fluid inclusion water in speleothems, Rapid Communications in Mass Spectrometry, 20, 2553-2558, 10.1002/rcm.2618, 2006.

Wadley, L.: What Stimulated Rapid, Cumulative Innovation After 100,000 Years Ago?, Journal of Archaeological Method and Theory, 28, 120-141, 10.1007/s10816-020-09499-y, 2021.

Wainer, K., Genty, D., Blamart, D., Daëron, M., Bar-Matthews, M., Vonhof, H., Dublyansky, Y., Pons-Branchu, E., Thomas, L., van Calsteren, P., Quinif, Y., and Caillon, N.: Speleothem record of the last 180 ka in Villars cave (SW France): Investigation of a large $\delta18O$ shift between MIS6 and MIS5, Quaternary Science Reviews, 30, 130-146, https://doi.org/10.1016/j.quascirev.2010.07.004, 2011.

Warken, S. F., Weissbach, T., Kluge, T., Vonhof, H., Scholz, D., Vieten, R., Schmidt, M., Winter, A., and Frank, N.: Last glacial millennial-scale hydro-climate and temperature changes in Puerto Rico constrained by speleothem fluid inclusion delta O-18 and delta H-2 values, Climate of the Past, 18, 167-181, 10.5194/cp-18-167-2022, 2022.

Wassenburg, J. A., Riechelmann, S., Schröder-Ritzrau, A., Riechelmann, D. F. C., Richter, D. K., Immenhauser, A., Terente, M., Constantin, S., Hachenberg, A., Hansen, M., and Scholz, D.: Calcite Mg and Sr partition coefficients in cave environments: Implications for interpreting prior calcite precipitation in speleothems, Geochimica et Cosmochimica Acta, 269, 581-596, https://doi.org/10.1016/j.gca.2019.11.011, 2020.

Wassenburg, J. A., Vonhof, H. B., Cheng, H., Martinez-Garcia, A., Ebner, P. R., Li, X. L., Zhang, H. W., Sha, L. J., Tian, Y., Edwards, R. L., Fiebig, J., and Haug, G. H.: Penultimate deglaciation Asian monsoon response to North Atlantic circulation collapse, Nature geoscience, 14, 937-+, 10.1038/s41561-021-00851-9, 2021.

Wortham, B. E., Montanez, I. P., Swart, P. K., Vonhof, H., and Tabor, C.: Variability in effective moisture inferred from inclusion fluid delta O-18 and delta H-2 values in a central Sierra Nevada stalagmite (CA), Quaternary Science Reviews, 279, 10.1016/j.quascirev.2022.107399, 2022.

Wurz, S.: Variability in the Middle Stone Age Lithic Sequence, 115,000–60,000 Years Ago at Klasies River, South Africa, Journal of Archaeological Science, 29, 1001-1015, https://doi.org/10.1006/jasc.2001.0799, 2002.
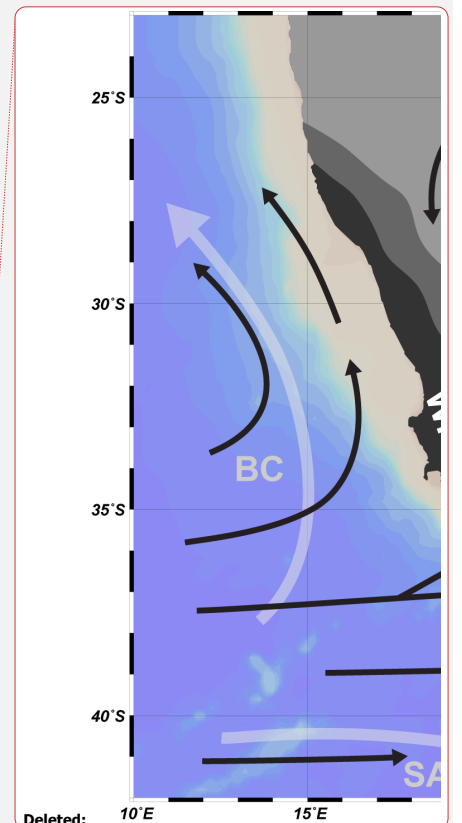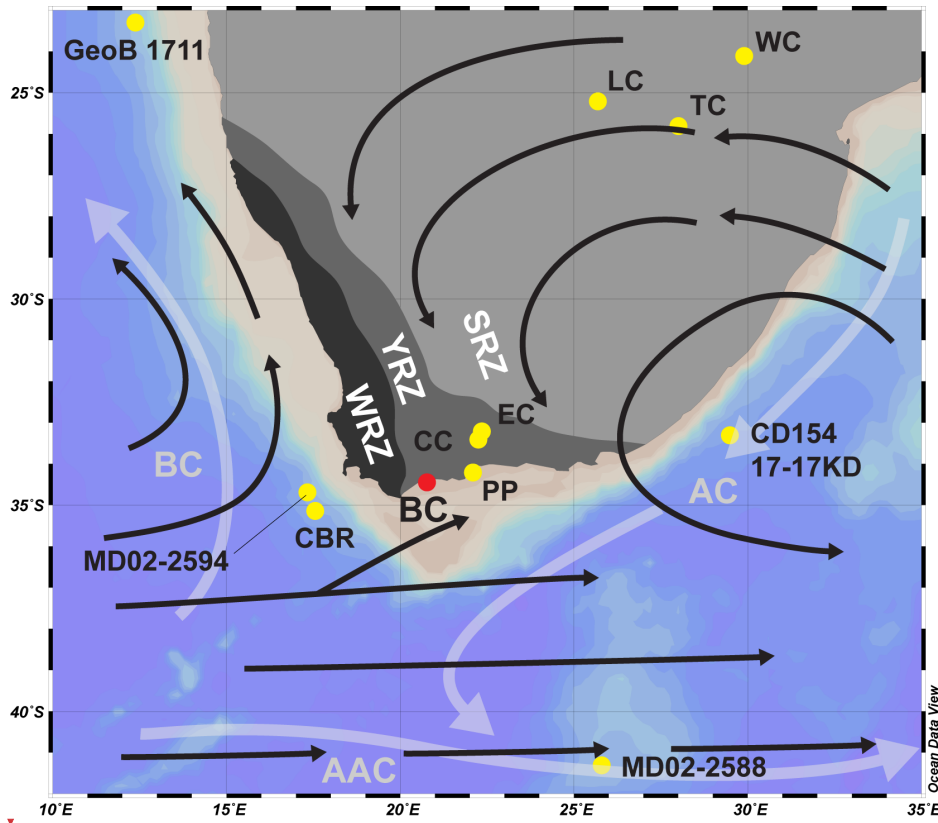
Figure 1. Map of southern Africa showing the study site (red circle) with the main rainfall zones (grey shading) and other sites referred to in the text (yellow circles). Major atmospheric circulation is indicated by thin black arrows and major oceanic currents are indicated by thick white arrows. BC - Blauwkrantz cave; WC - Wolkberg cave (Holkämper et al. 2009); LC - Lobatse cave (Holmgren et al. 1995); TC - Tswaing crater (Partridge et al. 1997); EC – Efflux Cave (Braun et al. 2020); CC – Cango Cave (Talma and Vogel 1992; Chase et al. 2021); PP – Pinnacle Point (Bar-Matthews et al. 2010). Marine cores MD02-2588; CD154 17-17K (Simon et al. (2013); GeoB 1711 (Kirst et al. 1999); MD02-2594 (Dyez et al. 2014) and CBR (Peeters et al. 2004). WRZ - Winter Rainfall Zone (dark grey); YRZ - Year-round Rainfall Zone (grey); SRZ - Summer Rainfall Zone (light grey); AC - Agulhas Current; BC - Benguela Current; SAC - South Atlantic Current.
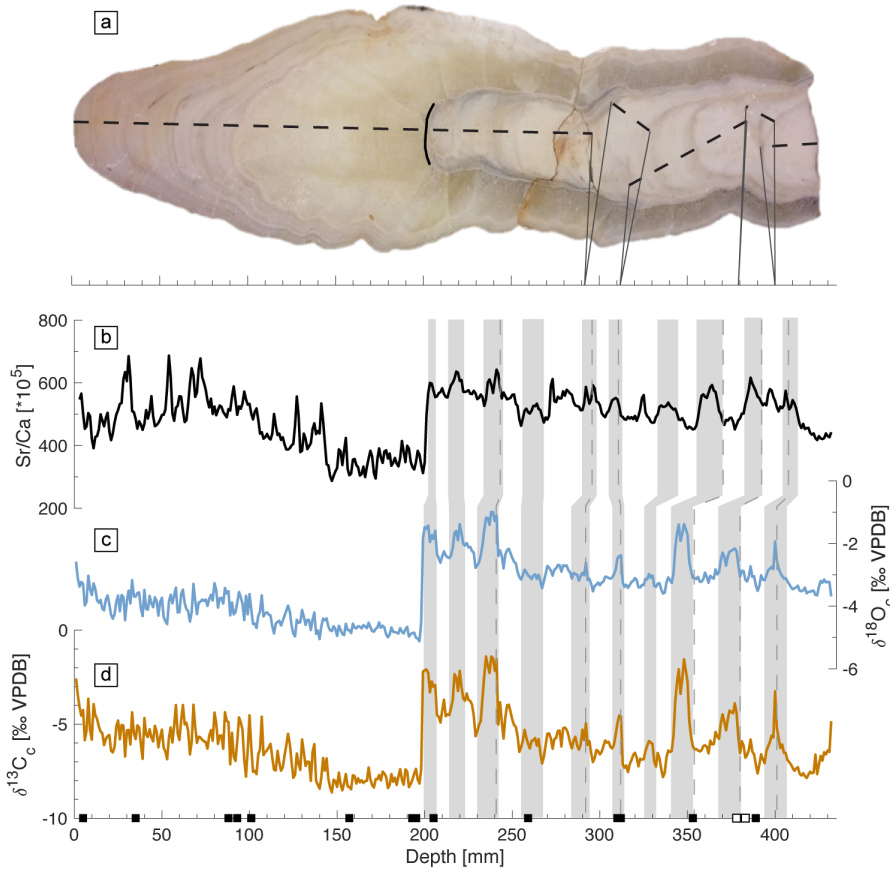
Figure 2: a. BL3 stalagmite. Dashed lines indicate the isotope transects along the main growth axes of the speleothem. The solid black line indicates the major hiatus between MIS 3 and the Holocene (see text). Sr/Ca and isotope analyses were measured on two different slabs resulting in slight offsets between the records (illustrated by the grey shadings). **b.** Sr/Ca as count-rate ratios from XRF scanning; **c.** $\delta^{18}O_c$; **d.** $\delta^{13}C_c$. Dashed lines indicate the onset of darker layers in the stalagmite. Dating depths are indicated by the black square symbols on the x-axis (the open symbols correspond to the two samples measured at the Isotope Laboratory at Xi'an Jiaotong University).
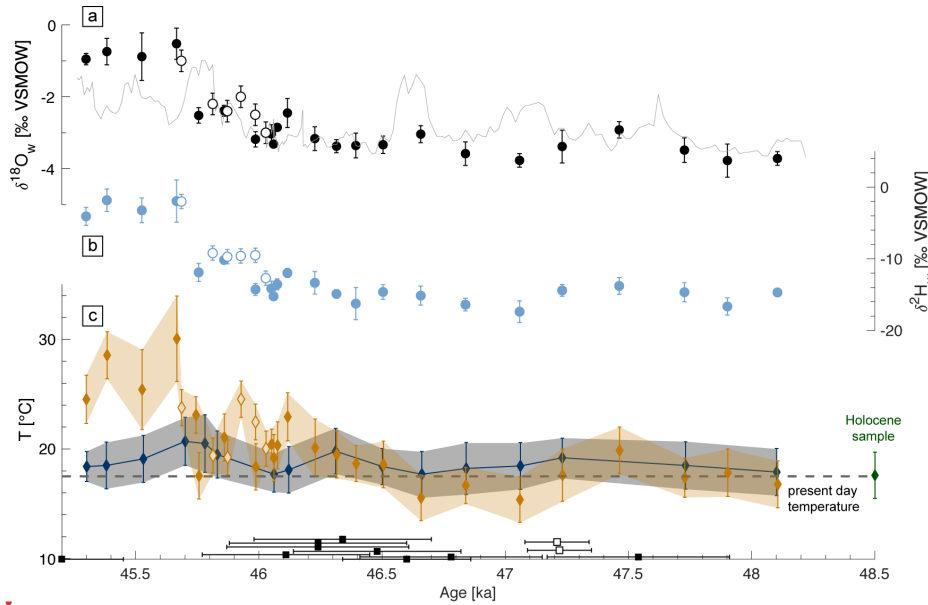
Figure 3: BL3 proxy data vs age. **a.** $\delta^{18}O_c$ (grey line) and $\delta^{18}O_w$ (black circles); **b.** δ^2H_w (light blue circles); **c.** Temperature reconstructions from fluid inclusion water isotopes (ochre diamonds) and microthermometry (dark blue line and diamonds). Open symbols correspond to samples analyzed at the University of Bern. In (c) the dashed line indicates the present-day temperature in the cave and the dark green diamond on the right corresponds to the topmost sample (microthermometry data). Black squares at the bottom indicates the U-Th dates and their associated error bars (2σ). The open square symbols correspond to the two samples measured at the Isotope Laboratory at Xi'an Jiaotong University.
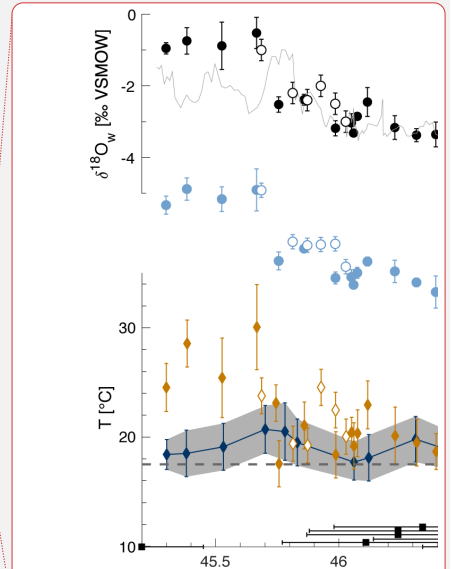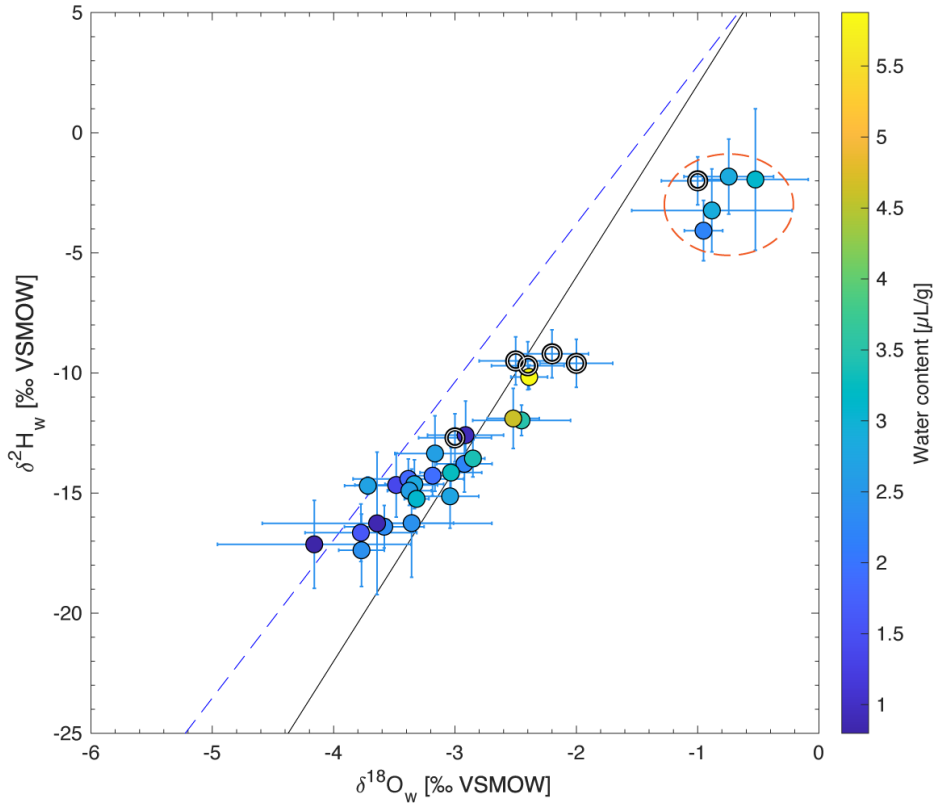
Figure 4: Fluid inclusion water isotope data plotted in δ^2H_w vs $\delta^{18}O_w$ space. Lines indicate the global (black) and local (dashed blue – from GNIP station at Cape Town airport from 1961 to 2013) meteoric water lines. The color bar on the right indicates the water content for each sample. The red dashed ellipse marks the youngest data cluster discussed in the text. Open symbols correspond to samples analyzed at the University of Bern. Error bars ± 1SD.

¶ ... [8]

¶
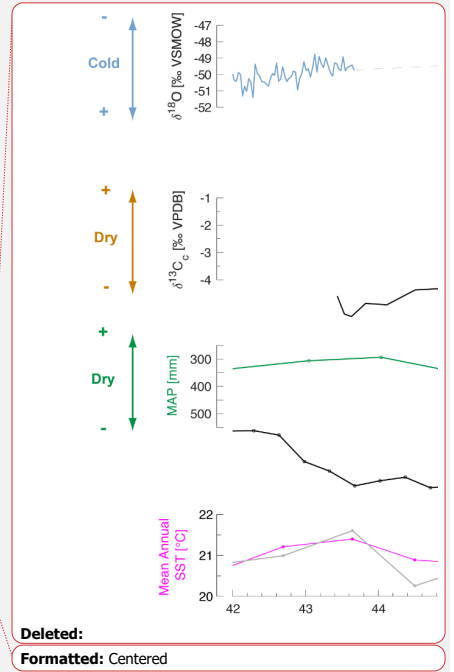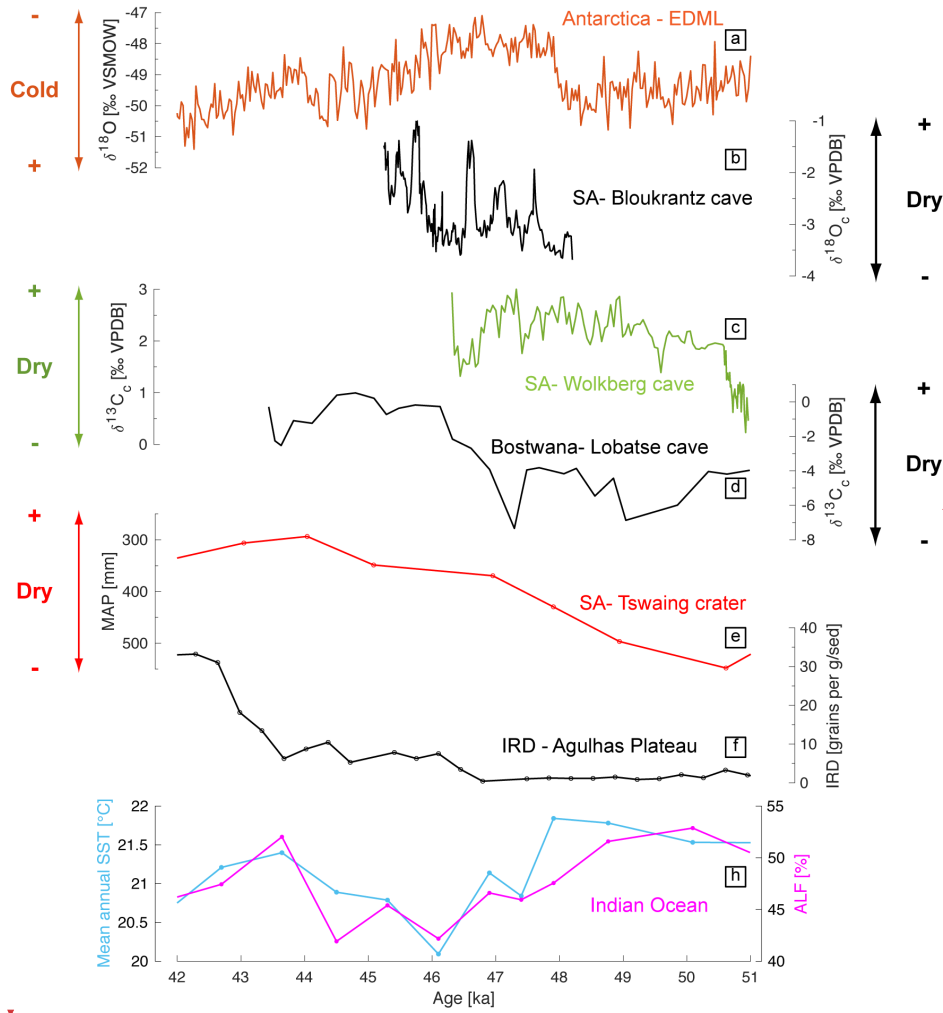
Figure 5: Comparison to other climate records: a. δ^{18}O from the EPICA Dronning Maud Land ice core in the Atlantic sector of the Antarctic Ice Sheet (EPICA community members 2006); b. δ^{18}Oc from Bloukrantz cave in the YRZ (this study); c. δ^{13}Cc from

Wolkberg cave in the SRZ (Holzkämper et al. 2009); d. $\delta^{13}Cc$ from Lobatse cave in the SRZ (Holmgren et al. 1995); e. Annual
140 precipitation reconstruction from Tswaing crater in the SRZ (Partridge et al. 1997); f. Ice Rafted Debris from core MD02-2588 on
the southern Agulhas Plateau (Simon et al. 2013); g. Mean annual Sea Surface Temperature and Agulhas Leakage Fauna
reconstructed from core CD154 17-17K in the southwest Indian Ocean (Simon et al. 2013).

Page 8: [1] Deleted   **Author**

Page 8: [1] Deleted   **Author**

Page 8: [2] Deleted   **Author**

Page 8: [2] Deleted   **Author**

Page 8: [2] Deleted   **Author**

Page 8: [2] Deleted   **Author**

Page 8: [2] Deleted   **Author**

Page 8: [2] Deleted   **Author**

Page 8: [2] Deleted   **Author**

Page 8: [2] Deleted   **Author**

Page 8: [2] Deleted   **Author**

Page 8: [2] Deleted   **Author**

Page 8: [2] Deleted   **Author**

Page 8: [2] Deleted   **Author**

Page 8: [2] Deleted   **Author**

Page 8: [2] Deleted   **Author**

Page 8: [2] Deleted	Author

Page 8: [2] Deleted	Author

Page 8: [3] Deleted	Author

Page 8: [3] Deleted	Author

Page 8: [3] Deleted	Author

Page 8: [3] Deleted	Author

Page 8: [3] Deleted	Author

Page 8: [3] Deleted	Author

Page 8: [3] Deleted	Author

Page 8: [3] Deleted	Author

Page 8: [4] Deleted	Author

Page 8: [4] Deleted	Author

Page 8: [4] Deleted	Author

Page 8: [4] Deleted	Author

Page 8: [4] Deleted	Author

Page 8: [4] Deleted	Author

Page 8: [5] Deleted   **Author**

Page 8: [5] Deleted   **Author**

Page 8: [5] Deleted   **Author**

Page 8: [6] Deleted   **Author**

Page 8: [6] Deleted   **Author**

Page 8: [6] Deleted   **Author**

Page 25: [7] Deleted   **Author**

Page 27: [8] Deleted   **Author**